

Journal of Geophysical Research: Oceans

RESEARCH ARTICLE

10.1002/2018JC013776

Special Section:

Sea State and Boundary Layer
Physics of the Emerging Arctic
Ocean

Key Points:

- An analysis of the measured wave attenuation shows a power law dependence on frequency with an exponent between two and four
- We show how to connect various dispersion equation models with a given power law, under the assumption of weak attenuation by a thin layer
- We show how energy loss mechanisms are connected to dispersion equations and power laws

Correspondence to:

M. H. Meylan,
mike.meylan@newcastle.edu.au

Citation:

Meylan, M. H., Bennetts, L. G., Mosig, J. E. M., Rogers, W. E., Doble, M. J., & Peter, M. A. (2018). Dispersion relations, power laws, and energy loss for waves in the marginal ice zone. *Journal of Geophysical Research: Oceans*, 123, 3322–3335. <https://doi.org/10.1002/2018JC013776>




Received 15 JAN 2018

Accepted 18 MAR 2018

Accepted article online 26 MAR 2018

Published online 10 MAY 2018

Dispersion Relations, Power Laws, and Energy Loss for Waves in the Marginal Ice Zone

M. H. Meylan¹ , L. G. Bennetts², J. E. M. Mosig³, W. E. Rogers⁴ , M. J. Doble⁵ , and M. A. Peter⁶

¹School of Mathematical and Physical Sciences, University of Newcastle, Newcastle, NSW, Australia, ²School of Mathematical Sciences, University of Adelaide, Adelaide, SA, Australia, ³Department of Mathematics and Statistics, University of Otago, Dunedin, New Zealand, ⁴Naval Research Laboratory, Stennis Space Center, MS, USA, ⁵Polar Scientific Ltd, Appin, UK, ⁶Institute of Mathematics, University of Augsburg, Germany and Augsburg Centre for Innovative Technologies, Augsburg, Germany

Abstract Analysis of field measurements of ocean surface wave activity in the marginal ice zone, from campaigns in the Arctic and Antarctic and over a range of different ice conditions, shows the wave attenuation rate with respect to distance has a power law dependence on the frequency with order between two and four. With this backdrop, the attenuation-frequency power law dependencies given by three dispersion relation models are obtained under the assumptions of weak attenuation, negligible deviation of the wave number from the open water wave number, and thin ice. It is found that two of the models (both implemented in WAVEWATCH III[®]), predict attenuation rates that are far more sensitive to frequency than indicated by the measurements. An alternative method is proposed to derive dispersion relation models, based on energy loss mechanisms. The method is used to generate example models that predict power law dependencies that are comparable with the field measurements.

1. Introduction

The marginal ice zone (MIZ) is the region of broken sea ice that forms at the boundary of the open and ice-covered oceans and is the region in which the ice cover is strongly affected by ocean surface waves and other open ocean processes. Most noteworthy is wave-induced breakup of large ice floes into smaller floes (Asplin et al., 2012; Collins et al., 2015; Kohout et al., 2015). Further, waves impact the ice cover by causing floes to collide (Martin & Becker, 1987; Yew et al., 2017), by increasing melt rates due to turbulence beneath floes (Wadhams et al., 1979), and by overwashing them (Massom & Stammerjohn, 2010; Skene et al., 2015).

The ice cover strongly affects the waves, causing them to attenuate with distance traveled, thus limiting breakup (and other impacts) to at most 100s of kilometers in from the open ocean (Kohout et al., 2014). Field measurements, going back more than forty years, have shown that waves typically attenuate exponentially and that the exponential attenuation rate is a function of wave period/frequency, with decreasing attenuation as the period increases (or the frequency decreases) (Meylan et al., 2014; Squire & Moore, 1980; Wadhams et al., 1988).

There are many applications which require an accurate model of wave attenuation in the MIZ. These include far more than just wave forecasting (which is obviously important), and we cannot model floe growth, floe size distribution, floe break up, or floe melting without an effective model of attenuation (Horvat & Tziperman, 2015). At present, we do not know the dominant mechanism that removes wave energy as it propagates in the MIZ, which is a major shortcoming in models. This lack of knowledge means that these models are speculative and require validation against field data (Bennetts et al., 2017).

Two model paradigms exist to understand wave attenuation. The first is wave scattering (e.g., Bennetts & Squire, 2012a; Kohout & Meylan, 2008; Montiel et al., 2016; Peter & Meylan, 2009), which conserves energy and in which attenuation results from an accumulation of scattering events produced by individual floes, where the floes are conventionally modeled as thin floating elastic plates (e.g., Bennetts & Williams, 2010; Meylan & Squire, 1994). Scattering models have been shown to agree reasonably well with experimental measurements (Bennetts & Squire, 2012b; Bennetts & Williams, 2015; Bennetts et al., 2010; Kohout & Meylan, 2008), but only when wavelengths are comparable to floe lengths. For waves appreciably longer than floes, scattering is negligible, and hence scattering models predict no attenuation, which is not supported by field data.

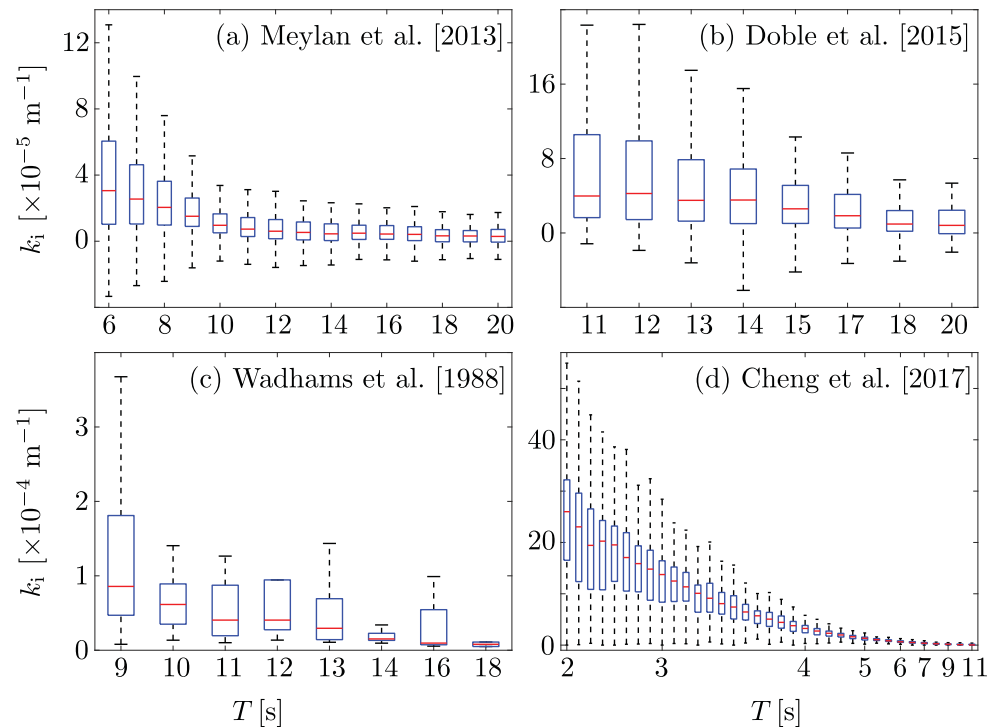


Figure 1. Box and whisker representations of the imaginary wave number component versus wave period, from field measurements, as reported by (a) Meylan et al. (1994), (b) Doble et al. (2015), (c) Wadhams et al. (1988), and (d) Cheng et al. (2017).

For waves much longer than floes—the so-called long-wavelength regime—attenuation is generally assumed to result from dissipation of wave energy, e.g., due to viscosity (Keller, 1998). In this regime, the modeling paradigm is that of an effective or homogenized ice layer, in which individual floes are not resolved. This paradigm leads to a dispersion relation linking the wave frequency and the complex wave number, where the imaginary component of the wave number defines the attenuation rate.

Recent field measurements (e.g., Cheng et al., 2017; Meylan et al., 2014), which are far more comprehensive than earlier experiments in terms of duration and extent, are predominantly in the long-wavelength regime. The measurements are used to tune model parameters, particularly the effective ice layer properties (e.g., Cheng et al., 2017). However, the functional dependence of the attenuation rate on frequency/period is dictated by the nature of the model and cannot be tuned. Therefore, in general, a model can only be tuned to match the data at a single frequency/period unless it has the correct functional dependence of attenuation on frequency.

In the present work, we begin by synthesizing analyses of key MIZ wave attenuation field measurements, showing a power law dependence of the average attenuation rate on frequency with order 2–4. We subsequently derive the attenuation-frequency power law dependence for three effective medium models (these are models which approximate the sea ice layer by an effective medium), using a perturbation method based on the observation that the change in length of long waves in the MIZ is negligible (Cheng et al., 2017, Figure 2). We find that only one model has order comparable to the field measurements, with the two other models giving far higher orders, i.e., they predict attenuation rates which are more sensitive to frequency than the measurements suggest. Moreover, we show how the attenuation rates predicted by the models can be derived based on energy loss principles, and we use this method to devise models with orders that fit the experimental measurements.

2. Field Measurements

We consider measurements made in the Arctic (Cheng et al., 2017; Wadhams et al., 1988) and Antarctic (Doble et al., 2015; Meylan et al., 2014), and in different seasons/ice conditions. The measurements have been reported previously, but most of the data analysis presented here is new. Measuring wave attenuation

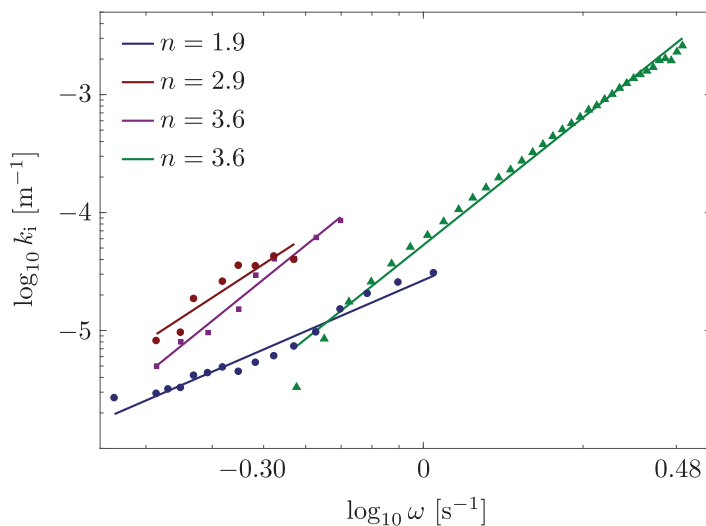


Figure 2. Log-log plots of median values of imaginary wave number components from Figure 1 versus angular frequency (markers), with best fits of form $k_i \propto \omega^n$ overlaid (lines): Meylan et al. (1994) (blue); Doble et al. (2015) (red); Wadhams et al. (1988) (magenta); and (d) Cheng et al. (2017) (green).

many measurements as possible and therefore do not distinguish between ice types, etc. This is because we aim to show that all the measured data show a roughly consistent power law relationship between attenuation and frequency (or period).

Two versions of attenuation are used. The first is based on wave energy E , and is written as

$$E(x; \omega) = E_0(\omega) e^{-\alpha x}, \quad (1)$$

where E_0 is the incident energy, α is the attenuation rate and x is the distance traveled, and the second is based on the wave amplitude A ,

$$A(x; \omega) = A_0(\omega) e^{-k_i x}, \quad (2)$$

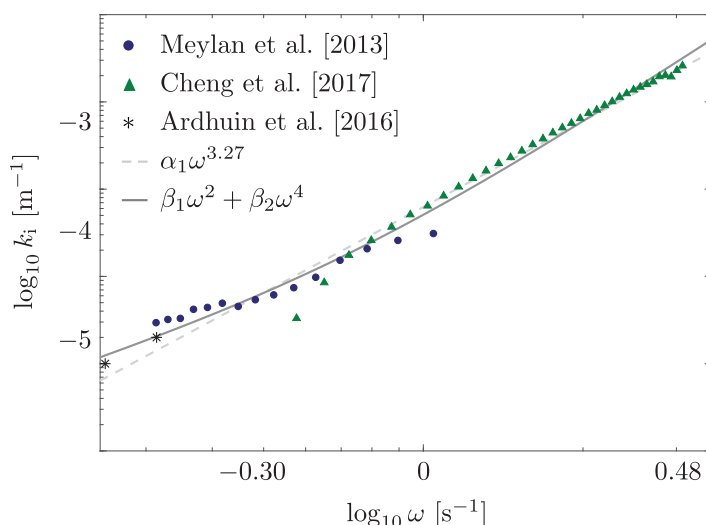


Figure 3. Log-log plot of median imaginary wave number versus angular frequency reported by Meylan et al. (1994) (blue bullets) and Cheng et al. (2017) (green triangles), with best fits to the combined data of the form $k_i = \alpha_1 \omega^n$ (light grey broken curve) and $k_i = \beta_1 \omega^2 + \beta_2 \omega^4$ (dark grey solid curve) overlaid. Imaginary wave number data reported by Arduin et al. [2016] are also included (*).

in the MIZ is challenging, requiring a series of measurements at different locations. Historical measurements (from the 1970s/1980s) reported by Wadhams et al. (1988) were not made simultaneously and this makes them liable to greater errors. We include them nevertheless, since they cover many field campaigns. More recently, technology has allowed drifting wave buoys making simultaneous measurements over long time periods which are relayed via satellite. These give much more accurate measurements and allow us to average, thus removing some of the problems caused by the evolution of the wave spectrum.

Interpretation of the wave data is complicated by a property of Fourier transforms and their inverse. In the context of measuring wave attenuation it means that to have accurate measurements of wave spectra, we require a long time measurement (so that the Fourier transform decomposition of the energy into frequencies is correct). However, for us to be able to interpret the change of wave energy between the two wave buoys requires an assumption of stationarity, which is likely to be violated if the measurements continue for too long. Each measurement should be seen as a sample from a random distribution, and only a process of averaging will give meaningful results. Meylan et al. (2014) showed that the median attenuation offers reliable results (a clear functional relationship between the attenuation rate and wave frequency). Further, we use as

where A_0 is the incident amplitude and the attenuation rate, k_i , is the imaginary component of the wave number in the MIZ, $k = k_r + i k_i$. Note that, since energy is proportional to amplitude squared, it follows that $\alpha = 2 k_i$. As is often the case, the amplitude formulation is more convenient mathematically, while the energy formulation is more easily interpreted from measurements. We will use the amplitude model here, meaning the measurements presented differ by a factor of half from those appearing in previous papers (where the results were based on energy).

Figure 1 shows box-and-whisker plots of the measured attenuation rates (k_i) versus wave period T . The data reported by Wadhams et al. (1988) summarized a series of campaigns in the late 1970s and early 1980s (many of which had been published previously), led by members of the Scott Polar Research Institute. The measurements are single data points, which were fitted to an exponential curve (even if the data did not support this due to spatial changing ice conditions, e.g., Squire & Moore [1980, Figure 4]). As noted above, the measurements were not made simultaneously and therefore suffer from noise, and moreover, they were made in highly variable ice conditions. Nevertheless, they represent almost ten years of fieldwork and are therefore worthy of evaluation. The measurements reported by Doble et al.

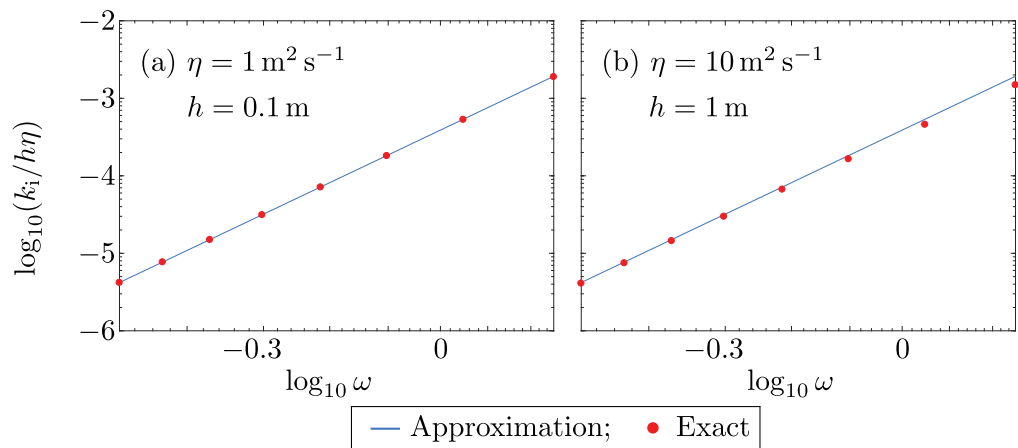


Figure 4. Log-log plot of scaled imaginary wave number versus angular frequency for the Keller (1998) model, for (a) $\eta = 1 \text{ m}^2 \text{ s}^{-1}$ and $h = 0.1 \text{ m}$, and (b) $\eta = 10 \text{ m}^2 \text{ s}^{-1}$ and $h = 1 \text{ m}$, with exact values (red bullets) and leading order approximation of equation (27) (blue lines).

(2015) were conducted in the Antarctic in pancake ice, and this was the first time wave buoys were deployed with on-board processing and satellite connectivity (such buoys have subsequently become the standard method to measure waves in the MIZ). The measurements reported by Meylan et al. (2014) were conducted in the Antarctic in broken ice floes. Figure 1a is almost identical of Meylan et al. (2014, Figure 4), noting that Kohout et al. (2014) present a different interpretation of the attenuation rate (based on the significant wave height). The measurements reported by Cheng et al. (2017) are taken from the recent sea-state cruise (Thomson et al., 2018). Cheng et al. (2017) performed an extensive analysis of the measurements, accounting for the effect of wind-generated waves and other processes. This allows the analysis of attenuation of short-period waves (high frequencies) without the roll-over effect dominating (Li et al., 2017). Further, the nature of the measurements in which the wave buoys were closely monitored gave these particular measurements unprecedented accuracy. Note that these measurements were made in pancake/frazil ice conditions so that even the short waves are much longer than the floe sizes.

Figure 2 shows log-log plots of the median attenuation rate versus angular frequency $\omega = 2\pi/T$. Straight line fits to each set of measurements are overlaid, and the slope of the lines determine a power law relationship of the form $k_i \sim \omega^n$. The n -values are given in the legend. While the attenuation magnitude is different for the four measurements, the power law order n varies from 1.9 to 3.6 only. Note that the attenuation rate in the pancake ice (Cheng et al., 2017; Doble et al., 2015) have different magnitudes but a similar order. The difference in the magnitude of the attenuation rates is likely to be due to differences in ice properties, especially ice thickness. The two lowest values of k_i for the Cheng et al. (2017) attenuation do not lie on the power law line. We do not know if this is real or the result of some error. We do note that the relative error is largely due to the small amount of energy at long periods.

Figure 3 shows the median values from the two most comprehensive data sets (Cheng et al., 2017; Meylan et al., 2014). The combined data displays a remarkable consistency, which can be approximated by the power law fit $k_i \sim \omega^{3.27}$, or, more accurately by a two-term fit of the form

$$k_i = \beta_1 \omega^2 + \beta_2 \omega^4, \quad (3)$$

which was first proposed by Meylan et al. (2014), and captures the attenuation rates for very long waves in the Arctic reported by Arduin et al. (2015). The two-term fit implies that there are two processes attenuating waves, one which is dominant for low frequencies (long periods) proportional to the frequency squared, and one which dominates at higher frequencies (shorter periods) proportional to frequency to the fourth power.

3. Dispersion Relations

In the deep open ocean, the standard dispersion relation for linear water waves (small steepnesses) is derived based on the assumptions of inviscid and incompressible water undergoing irrotational motions.

Let locations in the water domain be defined by the Cartesian coordinates (x, z) , for $x \in \mathbb{R}$ and $z < 0$. At the linearized free surface of the ocean, $z = 0$, kinematic and dynamic conditions are applied, where the kinematic condition enforces that water particles at the ocean surface remain there during wave motion, and the dynamic condition enforces pressure continuity between the water and atmosphere. The kinematic condition is expressed as

$$\left[\frac{\partial \phi}{\partial z} \right]_{z=0} = \frac{\partial \xi}{\partial t}, \quad (4)$$

where $\phi(x, z)$ is the velocity potential and $\xi(x)$ is the surface displacement. The dynamic condition is $p_{\text{wtr}} = p_{\text{atm}}$, where

$$p_{\text{wtr}}(\phi, \xi) = -\rho \left(\left[\frac{\partial \phi}{\partial t} \right]_{z=0} + g \xi \right) \quad \text{and} \quad p_{\text{atm}} \equiv 0, \quad (5)$$

where the water pressure is derived from the linearized version of Bernoulli's equation, with ρ the water density, and the zero atmospheric pressure is a standard normalization. Using the ansatzes

$$\phi = \frac{\omega A_0}{ik} e^{i(kx - \omega t) - kz} \quad \text{and} \quad \xi = A_0 e^{i(kx - \omega t)}, \quad (6)$$

and combining the kinematic and dynamic conditions, results in the open water dispersion relation

$$k \equiv k_0 = \frac{\omega^2}{g}, \quad (7)$$

relating the open water wave number $k_0 \in \mathbb{R}$ and the angular frequency ω . Note that we consider (infinitely) deep water. In the context of wave-ice interactions, it is standard to consider water of finite depth, leading to an infinite number of discrete solutions of the dispersion relation, where the wave modes supported by the other solutions are generated at inhomogeneities in the ice cover (e.g., an ice edge) and decay away from it (Fox & Squire, 1994; Wang & Shen, 2010). For our purpose of determining the dominant attenuation of long waves, the infinite depth assumption greatly simplifies the analysis, and in the MIZ the ocean is deep enough for this assumption to be valid.

Greenhill (1887) was the first to propose a modification of the open water dispersion relation for waves in the ice-covered ocean. He considered continuous (connected) ice cover, modeled as a thin-elastic plate, where *thin* implies that all displacements (and stresses and strains) in the ice can be derived from the vertical displacements at the interface with the water surface, ξ . The dynamic condition is modified to $p_{\text{wtr}} = p_{\text{plt}}$, in which p_{plt} is the plate pressure

$$p_{\text{plt}}(\xi) = \frac{1}{6} G (1 + \nu) h^3 \frac{\partial^2 \xi}{\partial x^4} + \rho h \frac{\partial^2 \xi}{\partial t^2}, \quad (8)$$

where the first term models an elastic response, with G the shear modulus and ν the Poisson ratio of the ice, and the second term models an inertial response, with ρ the ice density and h is the ice thickness. This results in the dispersion relation

$$\frac{G(1+\nu)h^3k^5}{6} - \rho h \omega^2 k + \rho g k = g \omega^2, \quad (9)$$

with wave number $k \in \mathbb{R}$, i.e., zero attenuation.

Fox and Squire (1992) extended the Greenhill (1887) model to include frictional viscous damping, based on the a model proposed by Robinson and Palmer (1990) for vibrations of the lids of storage drums of liquid, and hence referred to as the Robinson-Palmer model. The model was subsequently used by Vaughan et al. (2009) and Squire et al. (2009) to model wave attenuation of long wave components in the (quasi-continuous) Arctic basin, and by Bennetts and Squire (2012a) to model dissipation at the individual floe scale in the MIZ. Williams et al. (2013a, 2013b) used the Bennetts and Squire (2012a) model to parameterize wave attenuation in a wave-ice interaction model, designed for operational forecasting.

To our knowledge, Weber (1986) was the first to propose a dispersion relation for an effective MIZ ice cover, composed of many floes, under the long-wave assumption. He modeled the ice cover as a viscous layer,

and solved the resulting equations approximately under the auxiliary assumption that “the upper layer is so viscous it effectively halts the horizontal motion in the lower fluid layer at the interface.” Later, motivated by laboratory experiments of Newyear and Martin (1997) on wave attenuation through a layer of frazil ice, Keller (1998) derived a dispersion relation for a viscous ice layer without an auxiliary assumption. He treated the viscous layer as having finite thickness, i.e., nonthin, significantly complicating the analysis and increasing the number of wave modes supported. This was model was subsequently compared with the laboratory experiment (Newyear & Martin, 1999).

The Keller (1998) model has become arguably the most important effective ice layer model, with, notably, Wang and Shen (2010) extending it to include elasticity using a complex-valued viscosity (equivalent to a complex-valued shear modulus). In doing so they increased the difficulty of analyzing attenuation, in particular due to the mode-swapping phenomenon (Zhao et al., 2017). The Wang and Shen (2010) model has been integrated into WAVEWATCH III[®], along with a cognate version of the Greenhill (1887) model, using a complex-valued shear modulus, where it was referred to as the Fox-Squire model as it was a modification of the simpler model with real-valued shear modulus developed to describe reflection and transmission of ocean waves entering shore fast sea ice (Fox & Squire, 1994). Hereinafter, the modified Fox and Squire model will be labeled the Viscous-Greenhill model, acknowledging that it is a viscous version of the original Greenhill model.

Under the assumption of infinite depth, the dispersion relations can be written in the following form

$$D(\omega, k)(\omega^2 - gk(1 + Q(k, \omega))) = 0, \quad (10)$$

where D and Q are functions that appear when the dispersion relation is derived. We ignore roots due to the factor $D(\omega, k)$, as they lead to compressional or shear waves that are highly unlikely to be excited by surface gravity waves from the open ocean (Zhao et al., 2017), and noting that for a thin layer this term becomes a constant. We therefore write the dispersion equation as

$$\omega^2 = gk(1 + Q(k, \omega)). \quad (11)$$

In our analysis of the dispersion relations below, we assume that the change in the real part of the wave number (from the underlying open water wave number, k_0) is small, based on measurements reported by Cheng et al. (2017, Figure 2). Therefore, we require $Q(k_0, \omega)$ to be small, and write $\epsilon = Q(k_0, \omega) \ll 1$. We seek the wave number as a perturbation of the open-water wave number

$$k = k_0 + \epsilon k_1 + O(\epsilon^2), \quad (12)$$

and substituting into dispersion relation (11) gives the first-order perturbation as

$$\epsilon k_1 = -k_0 Q(k_0, \omega). \quad (13)$$

Therefore, the attenuation rate is

$$k_i \approx -\text{Im}\{k_0 Q(k_0, \omega)\}, \quad (14)$$

to first order in ϵ .

4. Energy Loss

It is instructive to consider the derivation of the attenuation directly from the energy loss mechanisms. It seems logical to start with an energy loss mechanism, exploiting the smallness of this loss, and to see if the subsequent power law dependence matches with measured results. The key to our derivation of energy loss is an assumption of small attenuation. This means that the potential and displacement can be expanded as

$$\phi = \phi_0 + \epsilon \phi_1 + O(\epsilon^2) \quad \text{and} \quad \xi = \xi_0 + \epsilon \xi_1 + O(\epsilon^2). \quad (15)$$

The zeroth-order potential and displacement have the same form as they do in open water (6), which we write as

$$\phi_0 = \frac{igA(x)}{\omega} e^{i(kx - \omega t) + kz} \quad \text{and} \quad \xi_0 = A(x) e^{i(kx - \omega t)}, \quad (16)$$

where $A(x)$ is the wave amplitude, which attenuates (slowly) over distance. Note that the surface is at $z = 0$ and the fluid occupies the region $z < 0$.

Let the rate of energy loss per unit distance, per unit time be denoted $R(x, t)$. In terms of an inner product $\langle \cdot \rangle$

$$2R(x, t) = \langle \sqrt{\mathcal{E}}(\phi, \xi)^T, \sqrt{\mathcal{E}}(\phi, \xi) \rangle = \langle \sqrt{\mathcal{E}}(\phi_0, \xi_0)^T, \sqrt{\mathcal{E}}(\phi_0, \xi_0) \rangle + \epsilon \langle \sqrt{\mathcal{E}}(\phi_1, \xi_1)^T, \sqrt{\mathcal{E}}(\phi_0, \xi_0) \rangle + \epsilon \langle \sqrt{\mathcal{E}}(\phi_0, \xi_0)^T, \sqrt{\mathcal{E}}(\phi_1, \xi_1) \rangle + O(\epsilon^2), \quad (17)$$

where T denotes transpose and \mathcal{E} is the energy loss operator (which must be self-adjoint and positive so we can therefore define its square root in the normal fashion). Note that we are using the complex form of the wave amplitude and potential so that, due to the conjugation in the inner product, we are averaging over time. Doing this makes energy proportional to the amplitude squared rather than half the amplitude squared, which is corrected for by introducing a factor of two on the left-hand side of equation (17). Note also that ξ is not an independent function of ϕ , so that there is only a single independent function on each side of the inner product, but we keep both ϕ and ξ for convenience and this expression for the inner product needs to be interpreted in this context. From (17), it follows that the zeroth-order energy loss (i.e., the dominant attenuation) can be calculated from the undisturbed wave, which will be illustrated by the concrete examples considered in sections 5 and 6.

We now consider the energy balance when the wave travels from x to $x + \Delta x$, assuming a small attenuation rate, and expressing the energy $E(x)$ (per unit of surface area) as

$$E = \rho g \frac{A^2}{2}.$$

The energy flux over Δx during a time step Δt is

$$E(x) c_g \Delta t - E(x + \Delta x) c_g \Delta t = R \Delta x \Delta t, \quad (18)$$

where c_g is the group velocity. Rearranging and taking the limit $\Delta x \rightarrow 0$ leads to the ordinary differential equation

$$\frac{dE}{dx} = -\frac{R}{c_g}. \quad (19)$$

The energy attenuation rate, α , is therefore

$$\alpha = \frac{R}{E c_g}, \quad (20)$$

and hence

$$k_i = \frac{R}{2 E c_g} = \frac{R}{\rho g A^2 c_g}. \quad (21)$$

In what follows, each model considered contains a free parameter, and the attenuation (or energy loss) is proportional to this parameter. For simplicity, we use the same symbol η in each model for this term, but it should be noted that this parameter has different dimensions in different models.

5. Models

5.1. Keller Model

For Keller's (1998) viscous-layer model $Q = Q_{\text{Kel}}$, where

$$Q_{\text{Kel}} = \frac{\rho}{\rho g k} \frac{S(kh)S(\chi h)\{N^4 - g^2 k^2 + 16\chi^2 \eta^4 k^6\} - 8i\chi \eta^2 k^3 N^2 \{1 - C(kh)C(\chi h)\}}{S(\chi h)\{gkS(kh) - N^2 C(kh)\} - 4i\chi \eta^2 k^3 S(kh)C(\chi h)}, \quad (22)$$

with

$$S(z) = \sinh z, \quad C(z) = \cosh z, \quad \chi^2 = k^2 - \frac{i \rho \omega}{\rho \eta}, \quad N = \omega + 2i k^2 \eta, \quad (23)$$

ρ the density of the viscous layer, and η the energy loss or viscosity parameter. In this case the viscosity parameter has the dimension of the kinematic viscosity of a fluid.

Let the thickness of the viscous ice layer, h , be small, such that $kh \ll 1$ and the Reynolds number $\omega h^2 \eta^{-1} \ll 1$, which implies that $|\chi h| \ll 1$. In these limits, Q_{Kel} reduces to

$$Q_{\text{Kel}}(k, \omega) = \frac{\rho}{\varrho} \frac{h^2 \omega^2 (\omega^2 + 4i k^2 \omega \eta) - k^2 h^2 g^2}{k^2 h^2 g^2 - g h (\omega^2 + 4i k^2 \omega \eta)}, \quad (24)$$

similarly to Keller's (1998) equation (29), and Wang and Shen's (2010) equation (57). It follows that

$$Q_{\text{Kel}}(k_0, \omega) = \frac{\rho}{\varrho} \frac{4i \omega^7 g^{-4} h^2 \eta}{h \omega^2 g^{-1} - h^2 \omega^4 g^{-2} + 4i \omega^5 g^{-3} h \eta}, \quad (25)$$

from which the imaginary component of the wave number is deduced to be

$$k_i \approx -\text{Im}\{k_0 Q_{\text{Kel}}(k_0, \omega)\} = \frac{\rho}{\varrho} \frac{4 \omega^9 g^{-5} h^2 \eta (h \omega^2 g^{-1} - h^2 \omega^4 g^{-2})}{(h \omega^2 g^{-1} - h^2 \omega^4 g^{-2})^2 + 16 \omega^{10} g^{-6} h^2 \eta^2}. \quad (26)$$

For values of the viscosity parameter, η , small such that $\eta \omega^3 g^{-2} \ll 1$, the attenuation coefficient can be expressed as a series in ω , with

$$k_i \approx \frac{4 \rho h \eta}{\varrho g^4} \omega^7 - \frac{4 \rho h^2 \eta}{\varrho g^5} \omega^9 + O(\omega^{11}), \quad (27)$$

where $k_0 h \ll 1$ has been used. Therefore, at leading order in frequency, Keller's (1998) attenuation coefficient is order 7, which is far more sensitive to frequency than field measurements of attenuation.

As an aside, note that the thin-limit dispersion relation given by equation (25) is equivalent to applying the standard kinematic condition (4) (as in Keller, 1998), along with the dynamic condition $p_{\text{wtr}} = p_{\text{Kel}}$, where

$$p_{\text{Kel}}(\xi) = \frac{h}{g} \left(\frac{\partial^4 \xi}{\partial t^4} + g^2 \frac{\partial^2 \xi}{\partial x^2} - 4 \eta \frac{\partial^5 \xi}{\partial t^3 \partial x^2} \right) \left(-\frac{\partial^2 \xi}{\partial t^2} + h g \frac{\partial^2 \xi}{\partial x^2} + 4 \eta \frac{\partial^3 \xi}{\partial t \partial x^2} \right)^{-1}. \quad (28)$$

Figure 4 shows log-log plots of the scaled attenuation rate versus frequency, for two different viscosity-thickness parameter combinations. Exact values of the imaginary component of the wave number (calculated numerically from the full dispersion relation) are shown, along with the leading order approximation (27). The approximation is accurate, even for the larger values of thickness and viscosity and high frequencies, thus indicating that the order 7 dependence of the attenuation rate is a general property of the Keller (1998) model for relevant parameters.

The leading-order attenuation rate in equation (27) can be derived using the energy loss method from section 4. For the Keller (1998) model, the energy loss is the product of the average velocity gradient squared, the layer thickness and the viscosity parameter. Since we have a thin layer we can approximate to first order the velocity gradient in the layer by the gradient at $z = 0$, and therefore

$$\sqrt{\mathcal{E}} = \sqrt{4 \rho h \eta} \left(\begin{array}{c} \frac{\partial}{\partial x} \frac{\partial}{\partial z} \\ 0 \end{array} \right)_{z=0}. \quad (29)$$

The rate of energy loss is given by

$$R = 2 \rho h \eta \left[\left(\frac{\partial^2 \phi}{\partial x \partial z} \right)_{z=0} \right]^2 = \frac{4 \rho h \eta}{2} A^2 g^2 k^4, \quad (30)$$

which gives the leading-order attenuation rate

$$k_i = \frac{R}{2 E c_g} = \frac{R}{\varrho g A^2 c_g} = \frac{4 \rho h \eta \omega g^2 k^4}{\varrho g^2} = \frac{4 \rho h \eta}{\varrho g^4} \omega^7, \quad (31)$$

as in equation (27).

5.2. Viscous-Greenhill Model

The Viscous-Greenhill model uses the dynamic condition $p_{\text{wtr}} = p_{\text{VG}}$, where

$$p_{\text{VG}}(\xi) = \frac{(G - i \omega \rho \eta) (1 + \nu) h^3}{6} \frac{\partial^4 \xi}{\partial x^4} + \rho h \frac{\partial^2 \xi}{\partial t^2}. \quad (32)$$

This gives dispersion relation (11) with $Q=Q_{VG}$, where

$$Q_{VG} = \frac{(G - i\omega\rho\eta)(1+\nu)h^3k^4 - 6\rho h\omega^2}{6\rho g}. \quad (33)$$

Therefore

$$Q_{VG}(k_0, \omega) = \frac{(G - i\omega\rho\eta)(1+\nu)h^3\omega^8/g^4 - 6\rho h\omega^2}{6\rho g}, \quad (34)$$

and the imaginary component of the wave number is

$$k_i \approx -\text{Im}\{k_0 Q_{VG}(k_0, \omega)\} = \frac{\rho\eta(1+\nu)h^3}{6\rho g^6} \omega^{11}. \quad (35)$$

This means that the attenuation rate predicted by the Viscous-Greenhill model is order 11, which is four orders of frequency more sensitive to frequency than the Keller (1998) model.

Figure 5 shows semi-log plots of the real component of the wave number scaled by the open water wave number (top plots), and log-log plots of the scaled attenuation rate (bottom) for the same two viscosity-thickness parameter combinations as in Figure 4, and for two values of the shear modulus. For the smaller values of viscosity and thickness (left-hand plots), the leading-order approximation (35) is accurate for the frequency range considered, and the real component of the wave number does not deviate from the open water wave number, i.e., $k_r/k_0 \approx 1$. For the larger values of viscosity and thickness (right), the approximation is less accurate, especially for the larger shear modulus, $G = 1$ GPa, and higher frequencies. The loss of accuracy of the approximation coincides with deviation of the real component of the wave number from the open water wave number, which means that it occurs in regimes not observed in the field measurements.

In terms of energy loss, for the Viscous-Greenhill model

$$\sqrt{\mathcal{E}} = \sqrt{\frac{\rho\eta(1+\nu)h^3}{6}} \begin{pmatrix} 0 & 0 \\ 0 & \frac{\partial}{\partial t} \frac{\partial^2}{\partial x^2} \end{pmatrix}, \quad (36)$$

so that the rate energy loss is

$$R = \frac{\rho\eta(1+\nu)h^3}{12} \left| \frac{\partial^3 \xi}{\partial t \partial x^2} \right|^2 = \frac{\rho\eta(1+\nu)h^3 A^2 \omega^2 k^4}{12}. \quad (37)$$

Therefore, the leading-order attenuation rate is

$$k_i = \frac{R}{2Ec_g} = \frac{R}{\rho g A^2 c_g} = \frac{\rho\eta(1+\nu)h^3 \omega^3 k^4}{6\rho g^2} = \frac{\rho\eta(1+\nu)h^3}{6\rho g^6} \omega^{11}, \quad (38)$$

as in equation (35).

5.3. Robinson–Palmer Model

The Robinson and Palmer (1990) model uses the dynamic condition $p_{wtr} = p_{RP}$, where

$$p_{RP}(\xi) = \frac{G(1+\nu)h^3}{6} \frac{\partial^4 \xi}{\partial x^4} + \rho h \frac{\partial^2 \xi}{\partial t^2} + \eta \frac{\partial \xi}{\partial t}, \quad (39)$$

in which η denotes a constant viscous damping force per unit area, per unit velocity. The resulting dispersion relation is such that $Q=Q_{RP}$, where

$$Q_{RP} = \frac{G(1+\nu)h^3k^4 - 6\rho h\omega^2 - 6i\omega\eta}{6\rho g}. \quad (40)$$

Therefore

$$Q_{RP}(k_0, \omega) = \frac{G(1+\nu)h^3\omega^8/g^4 - 6\rho h\omega^2 - 6i\omega\eta}{6\rho g}, \quad (41)$$

and the imaginary component of the wave number is

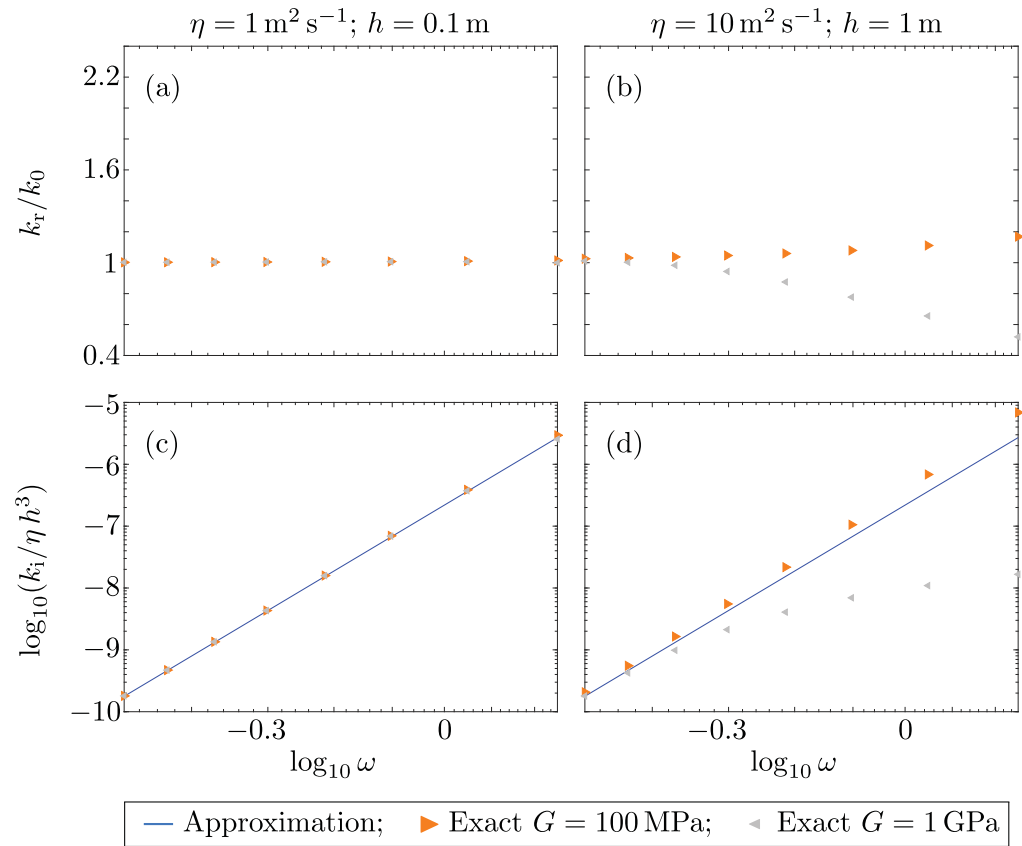


Figure 5. (a,b) Semi-log plot of scaled real wave number and (c,d) log-log plot of scaled imaginary wave number versus angular frequency for the Viscous-Greenhill model, for (a,c) $\eta = 1 \text{ m}^2 \text{ s}^{-1}$ and $h = 0.1 \text{ m}$, and (b,d) $\eta = 10 \text{ m}^2 \text{ s}^{-1}$ and $h = 1 \text{ m}$, with exact values (orange triangle right, $G = 100 \text{ Pa}$; silver triangle left, $G = 1 \text{ GPa}$) and leading order approximation of equation (35) (blue lines).

$$k_i \approx -\text{Im}\{k_0 Q_{RP}(k_0, \omega)\} = \frac{\eta}{\rho g^2} \omega^3. \quad (42)$$

This means that the attenuation rate predicted by the Robinson and Palmer (1990) model is order 3, which is comparable to the field measurements shown in section 2, although, in relation to the two-term approximation (3), over predicts sensitivity for low frequencies, and under predicts for high frequencies.

Figure 6 is similar to Figure 5 but for the Robinson and Palmer (1990) model. It provides cognate findings, with approximation (42) accurate for small viscosity and thickness, and less accurate for large viscosity and thickness, especially for large values of shear modulus and high frequencies, but that the loss of accuracy coincides with deviations in the real wave number component from the open water wave number, and is therefore outside the regime relevant for this investigation.

For the Robinson–Palmer model

$$\sqrt{\mathcal{E}} = \sqrt{\eta} \begin{pmatrix} 0 & 0 \\ 0 & \frac{\partial}{\partial t} \end{pmatrix}, \quad (43)$$

so that the rate of energy loss is

$$R = \frac{\eta}{2} \left| \frac{\partial \xi}{\partial t} \right|^2 = \frac{\eta A^2 \omega^2}{2}. \quad (44)$$

Therefore, the attenuation rate is

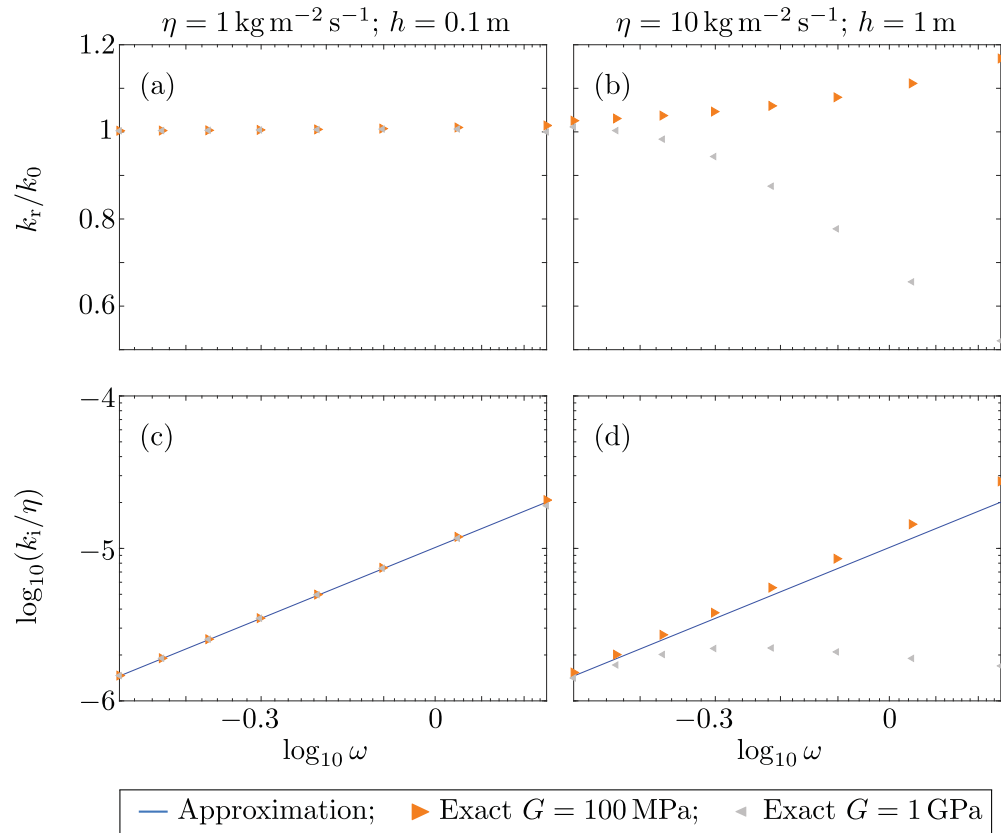


Figure 6. As in Figure 5 but for the Robinson and Palmer (1990) model.

$$k_i = \frac{R}{2 E c_g} = \frac{R}{\rho g A^2 c_g} = \frac{\eta}{\rho g^2} \omega^3, \quad (45)$$

as in equation (42).

6. Other Model Paradigms

There are many possible energy loss mechanisms and dispersion relations, which could be proposed to explain the observed attenuation power laws. We consider a few potential candidates, giving rise to power laws of order two and three.

6.1. Model With Order 2 Power Law

The first is one in which the energy loss is due to the product of the fluid pressure and velocity, so the energy loss is

$$\frac{\eta}{2} \left| \frac{\partial \xi}{\partial t} \left[\frac{\partial \phi}{\partial t} \right]_{z=0} \right|.$$

This energy loss is due to a phase shift between the fluid and surface ice motion. In this case, the energy loss operator is given by

$$\mathcal{E} = \eta \left(\begin{pmatrix} \left[\frac{\partial \phi}{\partial t} \right]_{z=0} & 0 \\ 0 & 1 \end{pmatrix}^* \begin{pmatrix} 0 & \frac{\partial}{\partial t} \\ 0 & 0 \end{pmatrix} \right), \quad (46)$$

where the star denotes the adjoint operator. Therefore, the rate of energy loss is

$$R = \frac{\eta A^2 g \omega}{2}, \quad (47)$$

and the attenuation rate is

$$k_i = \frac{R}{2 E c_g} = \frac{R}{\rho g A^2 c_g} = \frac{\eta}{\rho g} \omega^2. \quad (48)$$

The equivalent dispersion equation has the dynamic condition $p_{\text{wtr}} = p_{\text{mod}-2}$, where

$$p_{\text{mod}-2}(\xi) = -i \eta \left[\frac{\partial \phi}{\partial t} \right]_{z=0}. \quad (49)$$

Note that the idea of imaginary pressure is simply to represent the phase shift and this expression can only be thought of in the context of the frequency domain. This results in the dispersion relation

$$\omega^2 = g k \left(1 + \frac{i \eta \omega^2}{\rho g k} \right), \quad (50)$$

which gives an attenuation rate, k_i , that agrees with equation (48).

6.2. Model With Order 3 Power Law

We propose a different model to that of Robinson and Palmer (1990) that provides order three dependence, and with additional dependence on thickness. We assume that the energy loss is due to the square of the horizontal velocity times the thickness, i.e.,

$$h \left[\left[\frac{\partial \phi}{\partial x} \right]_{z=0} \right]^2.$$

We believe that this model is likely to be more widely applicable than the Robinson–Palmer model, as it provides dependence of the attenuation rate on ice thickness (Doble et al., 2015). The horizontal ice velocity squared represents the energy transferred to the ice by the fluid and we propose here that energy loss may be proportional to this. In this case the energy loss operator is given by

$$\sqrt{\mathcal{E}} = \sqrt{h \eta} \begin{pmatrix} \left[\frac{\partial \phi}{\partial x} \right]_{z=0} & 0 \\ 0 & 1 \end{pmatrix}. \quad (51)$$

Therefore, the rate of energy loss is

$$R = \frac{h \eta A^2}{2} \times \frac{g^2 k^2}{\omega^2}, \quad (52)$$

and the attenuation rate is

$$k_i = \frac{R}{2 E c_g} = \frac{R}{\rho g A^2 c_g} = \frac{h \eta}{\rho g^2} \omega^3. \quad (53)$$

The equivalent dispersion equation uses the dynamic equation $p_{\text{wtr}} = p_{\text{mod}-3}$, where

$$p_{\text{mod}-3}(\xi) = h \eta \left[\frac{\partial \phi}{\partial z} \right]_{z=0}. \quad (54)$$

This results in the dispersion equation

$$\omega^2 = g k \left(1 + \frac{i h \eta \omega}{\rho g} \right), \quad (55)$$

which gives a k_i that agrees with equation (53).

7. Conclusions

We have made two observations. The first is that the field measurements show a clear power law relationship between attenuation and frequency with a coefficient of between two and four. The second is that dispersion equation models for wave attenuation, under the assumptions of deep water and small

attenuation, also give rise to power law relations. Based on these two observations, we proposed the key idea that the dispersion relation models have associated energy loss models, which can be used to determine the power law relationship or to engineer a desired relationship. We believe that the two observations and the energy loss model will be of significant use in understanding wave attenuation in the MIZ. We conclude that measurements of wave attenuation should be fitted to power laws, that only models which have reasonable power law behavior should be used, and that the energy loss mechanism should be found to match the experimentally observed power laws.

Acknowledgments

M.H.M., L.G.B., J.E.M.M., and M.A.P. thank the Isaac Newton Institute for Mathematical Sciences for support and hospitality during the program Mathematics of Sea Ice Phenomena when work on this paper was undertaken, with support by EPSRC (grant number EP/K032208/1). M.H.M. and L.G.B. were also partially supported by a grant from the Simons Foundation. This work was supported by the Office of Naval Research Code 322, *Arctic and Global Prediction*, directed by Martin Jeffries and Scott Harper. Grants: Meylan, N000141512611; Mosig N00014-131-0279 Doble, N000141310290; Rogers, N0001413WX20825. The data used in this study can be found in a table in Wadhams et al. (1988) and in links provided in Meylan et al. (2014), Doble et al. (2015), and Cheng et al. (2017).

References

- Ardhuin, F., Collard, F., Chapron, B., Girard-Ardhuin, F., Guitton, G., Mouche, A., & Stopa, J. E. (2015). Estimates of ocean wave heights and attenuation in sea ice using the SAR wave mode on Sentinel-1A. *Geophysical Research Letters*, 42, 2317–2325. <https://doi.org/10.1002/2014GL062940>
- Ardhuin, F., Sutherland, P., Doble, M. J., & Wadhams, P. (2016). Ocean waves across the Arctic: Attenuation due to dissipation dominates over scattering for periods longer than 19s. *Geophysical Research Letters*, 43, 5775–5783. <https://doi.org/10.1002/2016GL068204>
- Asplin, M. G., Galley, R., Barber, D. G., & Prinsenberg, S. (2012). Fracture of summer perennial sea ice by ocean swell as a result of Arctic storms. *Journal of Geophysical Research*, 117, C06025. <https://doi.org/10.1029/2011JC007221>
- Bennetts, L. G., O'farrell, S., & Uotila, P. (2017). Impacts of ocean-wave-induced breakup of Antarctic sea ice via thermodynamics in a stand-alone version of the CICE sea-ice model. *Cryosphere*, 11(3), 1035–1040. <https://doi.org/10.5194/tc-11-1035-2017>
- Bennetts, L. G., Peter, M. A., Squire, V. A., & Meylan, M. H. (2010). A three-dimensional model of wave attenuation in the marginal ice zone. *Journal of Geophysical Research*, 115, C12043. <https://doi.org/10.1029/2009JC005982>
- Bennetts, L. G., & Squire, V. A. (2012a). On the calculation of an attenuation coefficient for transects of ice-covered ocean. *Proceedings of the Royal Society A*, 468, 136–162. <https://doi.org/10.1098/rspa.00000000>
- Bennetts, L. G., & Squire, V. A. (2012b). Model sensitivity analysis of scattering-induced attenuation of ice-coupled waves. *Ocean Modelling*, 45–46, 1–13. <https://doi.org/10.1016/j.ocemod.2012.01.002>
- Bennetts, L. G., & Williams, T. D. (2010). Wave scattering by ice floes and polynyas of arbitrary shape. *Journal of Fluid Mechanics*, 662, 5–35.
- Bennetts, L. G., & Williams, T. D. (2015). Water wave transmission by an array of floating disks. *Proceedings of the Royal Society A*, 471, 20140698. <https://doi.org/10.1098/rspa.2014.0698>
- Cheng, S., Rogers, W. E., Thomson, J., Smith, M., Doble, M. J., Wadhams, P., et al. (2017). Calibrating a viscoelastic sea ice model for wave propagation in the Arctic fall marginal ice zone. *Journal of Geophysical Research: Oceans*, 122, 8770–8793. <https://doi.org/10.1002/2017JC013275>
- Collins, C. O., Rogers, W. E., Marchenko, A., & Babanin, A. V. (2015). In situ measurements of an energetic wave event in the arctic marginal ice zone. *Geophysical Research Letters*, 42, 1863–1870. <https://doi.org/10.1002/2015GL063063>
- Doble, M. J., Carolis, G. D., Meylan, M. H., Bidlot, J.-R., & Wadhams, P. (2015). Relating wave attenuation to pancake ice thickness, using field measurements and model results: Waves in pancakes. *Geophysical Research Letters*, 42, 4473–4481. <https://doi.org/10.1002/2015GL063628>
- Fox, C., & Squire, V. A. (1994). On the oblique reflexion and transmission of ocean waves at shore fast sea ice. *Philosophical Transactions of the Royal Society A*, 347, 185–218.
- Greenhill, A. (1887). Wave motion in hydrodynamics. *American Journal of Mathematics*, 9, 62–112.
- Horvat, C., & Tziperman, E. (2015). A prognostic model of the sea ice floe size and thickness distribution. *Cryosphere*, 9, 2119–2134. <https://doi.org/10.5194/tcd-9-2955-2015>
- Keller, J. B. (1998). Gravity waves on ice-covered water. *Journal of Geophysical Research*, 103, 7663–7669.
- Kohout, A. L., & Meylan, M. H. (2008). An elastic plate model for wave attenuation and ice floe breaking in the marginal ice zone. *Journal of Geophysical Research*, 113, C09016. <https://doi.org/10.1029/2007JC004434>
- Kohout, A. L., Williams, M. J. M., Dean, S. M., & Meylan, M. H. (2014). Storm-induced sea-ice breakup and the implications for ice extent. *Nature*, 509(7502), 604–607. <https://doi.org/10.1038/nature13262>
- Kohout, A. L., Williams, M. J. M., Toyota, T., Lieser, J., & Hutchings, J. (2015). In situ observations of wave-induced sea ice breakup. *Deep-Sea Research Part II*, 131, 22–27. <https://doi.org/10.1016/j.dsr2.2015.06.010>
- Li, J., Kohout, A. L., Doble, M. J., Wadhams, P., Guan, C., & Shen, H. H. (2017). Rollover of apparent wave attenuation in ice covered seas. *Journal of Geophysical Research: Oceans*, 122, 8557–8566. <https://doi.org/10.1002/2017JC012978>
- Martin, S., & Becker, P. (1987). High-frequency ice floe collisions in the Greenland Sea during the 1984 marginal ice zone experiment. *Journal of Geophysical Research*, 92, 7071–7084.
- Massom, R. A., & Stammerjohn, S. E. (2010). Antarctic sea ice change and variability: Physical and ecological implications. *Polar Science*, 4(2), 149–186. <https://doi.org/10.1016/j.polar.2010.05.001>
- Meylan, M. H., Bennetts, L. G., & Kohout, A. L. (2014). In situ measurements and analysis of ocean waves in the Antarctic marginal ice zone. *Geophysical Research Letters*, 41, 5046–5051. <https://doi.org/10.1002/2014GL060809>
- Meylan, M. H., & Squire, V. A. (1994). The response of ice floes to ocean waves. *Journal of Geophysical Research*, 99, 891–900.
- Montiel, F., Squire, V. A., & Bennetts, L. G. (2016). Attenuation and directional spreading of ocean wave spectra in the marginal ice zone. *Journal of Fluid Mechanics*, 790, 492–522. <https://doi.org/10.1017/jfm.2016.21>
- Newyear, K., & Martin, S. (1997). A comparison of theory and laboratory measurements of wave propagation and attenuation in grease ice. *Journal of Geophysical Research*, 102, 25,091–25,099.
- Newyear, K., & Martin, S. (1999). Comparison of laboratory data with a viscous two-layer model of wave propagation in grease ice. *Journal of Geophysical Research*, 104, 7837–7840. <https://doi.org/10.1029/1999JC900002>
- Peter, M. A., & Meylan, M. H. (2009). Water-wave scattering by vast fields of bodies. *SIAM Journal on Applied Mathematics*, 70(5), 1567–1586.
- Robinson, N. J., & Palmer, S. C. (1990). A modal analysis of a rectangular plate floating on an incompressible liquid. *Journal of Sound and Vibration*, 142, 453–460.
- Skene, D. M., Bennetts, L. G., Meylan, M. H., & Toffoli, A. (2015). Modelling water wave overwash of a thin floating plate. *Journal of Fluid Mechanics*, 777, R3. <https://doi.org/10.1017/jfm.2015.378>
- Squire, V. A., & Fox, C. (1992). On ice coupled waves: a comparison of data and theory. In Murthy, T. K., Sackinger, W. M., Wadhams P. (Eds.), *Advances in ice technology: Proc. 3rd Int. Conf. on Ice Technology*. Cambridge, MA.

- Squire, V., & Moore, S. C. (1980). Direct measurement of the attenuation of ocean waves by pack ice. *Nature*, 283(5745), 365–368.
- Squire, V. A., Vaughan, G. L., & Bennetts, L. G. (2009). Ocean surface wave evolution in the Arctic Basin. *Geophysical Research Letters*, 36, L22502. <https://doi.org/10.1029/2009GL040676>
- Thomson, J., Ackley, S., Girard-Ardhuin, F., Ardhuin, F., Babanin, A., Bidlot, G., et al. (2018). Overview of the arctic sea state and boundary layer physics program. *Journal of Geophysical Research: Oceans*. <https://doi.org/10.1002/2018JC013766>, in press.
- Vaughan, G. L., Bennetts, L. G., & Squire, V. A. (2009). The decay of flexural-gravity waves in long sea ice transects. *Proceedings of the Royal Society A*, 465, 2785–2812. <https://doi.org/10.1098/rspa.2009.0187>
- Wadhams, P., Gill, A. E., & Linden, P. F. (1979). Transects by submarine of the East Greenland Polar Front. *Deep-Sea Research*, 26(A), 1311–1327.
- Wadhams, P., Squire, V. A., Goodman, D. J., Cowan, A. M., & Moore, S. C. (1988). The attenuation rates of ocean waves in the marginal ice zone. *Journal of Geophysical Research*, 93, 6799–6818.
- Wang, R., & Shen, H. H. (2010). Gravity waves propagating into an ice-covered ocean: A viscoelastic model. *Journal of Geophysical Research*, 115, C06024. <https://doi.org/10.1029/2009JC005591>
- Weber, J. E. (1986). Wave attenuation and wave drift in the marginal ice zone. *Journal of Physical Oceanography*, 17, 2351–2361.
- Williams, T. D., Bennetts, L. G., Squire, V. A., Dumont, D., & Bertino, L. (2013a). Wave-ice interactions in the marginal ice zone. Part 1: Theoretical foundations. *Ocean Modelling*, 71, 81–91. <https://doi.org/10.1016/j.ocemod.2013.05.010>
- Williams, T. D., Bennetts, L. G., Squire, V. A., Dumont, D., & Bertino, L. (2013b). Wave-ice interactions in the marginal ice zone. Part 2: Numerical implementation and sensitivity studies along 1D transects of the ocean surface. *Ocean Modelling*, 71, 92–101. <https://doi.org/10.1016/j.ocemod.2013.05.011>
- Yiew, L. J., Bennetts, L. G., Meylan, M. H., Thomas, G. A., & French, B. J. (2017). Wave-induced collisions of thin floating disks. *Physics of Fluids*, 29(12), 127102. <https://doi.org/10.1063/1.5003310>
- Zhao, X., Cheng, S., & Shen, H. H. (2017). Nature of wave modes in a coupled viscoelastic layer over water. *Journal of Engineering Mechanics*, 143(10), 04017,114, [https://doi.org/10.1061/\(ASCE\)EM.1943-7889.0001332](https://doi.org/10.1061/(ASCE)EM.1943-7889.0001332)